Field Verification of ADCP Surface Gravity Wave Elevation Spectra

A. J. F. HOITINK

Hydrology and Quantitative Water Management Group, Wageningen University, Wageningen, and Institute for Marine and Atmospheric Research Utrecht, Utrecht University, Utrecht, Netherlands

H. C. PETERS

North Sea Directorate, Rijkswaterstaat, Netherlands

M. SCHROEVERS

National Institute for Coastal and Marine Management/RIKZ, Rijkswaterstaat, Netherlands

(Manuscript received 22 November 2005, in final form 9 August 2006)

ABSTRACT

Acoustic Doppler current profilers (ADCPs) can measure orbital velocities induced by surface gravity waves, yet the ADCP estimates of these velocities are subject to a relatively high noise level. The present paper introduces a linear filtration technique to significantly reduce the influence of noise and turbulence from energy spectra of combined orbital velocity measurements. Data were collected in 13-m-deep water with a 1.2-MHz ADCP sampling in mode 12, where a collocated wave buoy was used for verification. The surface elevation spectra derived from the filtrated and nonfiltrated measurements were compared with corresponding wave buoy spectra. In the frequency range between 0.12 and 0.5 Hz, ADCP- and wave-buoy-derived spectral estimates matched very well, even without applying the filtration technique. At frequencies below 0.12 Hz, the ADCP-derived surface elevation spectra are biased, caused by a depth-varying excess of spectral energy density in the measured orbital velocities, peaking at middepth. Internal waves may provide an explanation for the energy excess, as the experiment was conducted in the region of influence of the Rhine freshwater plume. Alternatively, infragravity waves may be the cause of the depth variation of low-frequency spectral energy density.

1. Introduction

Conventional wave gauges for continuous monitoring of sea and swell in shelf seas include heave-pitch-and-roll buoys (Longuet-Higgins et al. 1963) and fixed instruments like pressure sensor–current meter (PUV) combinations (Nagata 1964; Bowden and White 1966) and step gauges. The collective disadvantage of those systems is that they are located in the upper part of the water column or even tower above the water surface, which creates hindrance for navigation and renders the instruments susceptible for physical damage caused by, for example, fishing boats and floating debris or ice. An acoustic Doppler current profiler (ADCP) can measure directional spectra of sea and swell by looking upward from the seafloor. Based on a field intercomparison between a 1.2-MHz broadband ADCP and a collocated Datawell Waverider buoy in 13-m-deep water, the present paper demonstrates the potential of broadband ADCPs for shelf sea wave measurement, focusing on nondirectional surface elevation spectra.

There have been extensive studies addressing the measurement of surface elevation spectra using acoustic Doppler velocity measurements. Based on a comparison with a collocated array of pressure transducers in 7-m-deep water, Herbers et al. (1991) established that a single-range (1 m) coherent Doppler sonar system with four acoustic beams inclined 45° from the vertical achieved a spectral noise level as low as 0.1 $(\text{cm s}^{-1})^2\ \text{Hz}^{-1}$. Bottom pressure derived from velocity measurements and linear theory, as well as cospectra of pressure and velocity, were in excellent agreement with corresponding spectra based on measurements from the pressure array.

Corresponding author address: A. J. F. Hoitink, Hydrology and Quantitative Water Management Group, Department of Environmental Sciences, Wageningen University, Droevendaalsesteeg 4, P.O. Box 47, 6700 AA Wageningen, Netherlands.
E-mail: ton.hoitink@wur.nl

DOI: 10.1175/JTECH2000.1

© 2007 American Meteorological Society

Krogstad et al. (1988) presented a comparison of directional wave data from a range-gated acoustic Doppler current meter (ADCM) and a PUV. Despite high noise levels in the ADCM, exceeding 50 $(\text{cm s}^{-1})^2$ Hz^{-1}, peak directions and directional spread agreed reasonably. The velocity error was a limitation inherent to incoherent processing of Doppler sonar (Theriault 1986). Compared to coherent systems (Lhermitte and Serafin 1984), incoherent (or narrowband) systems allow for range gating without compromising sampling frequency, which is particularly relevant to measurement of orbital wave velocities. Broadband Doppler sonar combines aspects of incoherent and coherent Doppler sonar processing techniques. For broadband systems, range gating is feasible without compromising the sampling frequency, whereas the spatial resolution and velocity variance that can be achieved is in between the two methods that the system is based upon (Brumley et al. 1983).

Apart from wave orbital velocity and instrumental noise, shelf sea ADCP measurements are subject to turbulence-induced velocity fluctuation, mixed layer oscillations, tidal, and subtidal flows. For wave analysis purposes, subseries typically cover 20 min or less, and the tidal and subtidal components can be readily isolated. In this paper a method is introduced that separates noise and turbulence-induced velocity fluctuations in a linear combination of high-pass-filtered ADCP measurements of wave orbital velocities. This is outlined in section 2, which is followed by a description of the field experiment and data processing in section 3. Section 4 compares surface elevation spectra derived from the processed ADCP measurements with corresponding spectra from wave buoy measurements. Sections 5 and 6 conclude this paper with a discussion and conclusions.

2. Theoretical approach

A coordinate system is defined with the origin corresponding to the ADCP's central vertical axis. The x and y coordinate axes correspond with positive velocity components u and v (respectively), and z and w are measured positively upward. The origin of z is at the burst-averaged sea level. The four along-beam velocity components u_1, u_2, v_1, and v_2 are a weighted sum of the local horizontal and vertical velocity, according to

$$u_1(d, 0, z) = u(d, 0, z)\sin\alpha + w(d, 0, z)\cos\alpha, \quad (1)$$

$$u_2(-d, 0, z) = -u(-d, 0, z)\sin\alpha + w(-d, 0, z)\cos\alpha, \quad (2)$$

$$v_1(0, d, z) = v(0, d, z)\sin\alpha + w(0, d, z)\cos\alpha, \quad (3)$$

$$v_2(0, -d, z) = -v(0, -d, z)\sin\alpha + w(0, -d, z)\cos\alpha, \quad (4)$$

where α is the angle between the central axis and the four beams. The horizontal distance d between the central vertical axis and four depth cells at an equal elevation z is defined by

$$d = (z + h - T)\tan\alpha, \quad (5)$$

where h is water depth and T is the height of the transducer above the bed. A horizontal velocity component disposed of oscillations at tidal and subtidal frequencies u can be separated into contributions of wave-induced $\tilde{u}$ and turbulence components u':

$$u = \tilde{u} + u'. \quad (6)$$

Similar expressions hold for v, w and $u_{1,2}$ and $v_{1,2}$. Apart from turbulence, instrumental noise also contributes to the fluctuating component. The wave-induced water surface displacement $\eta(t)$ at the central vertical axis is given by

$$\tilde{\eta}(t) = \int_{-\infty}^{\infty}\int_{-\pi}^{\pi} F(\omega, \theta)e^{i(\omega t - \phi)}\, d\theta\, d\omega, \quad (7)$$

where $F(\omega, \theta)$ is the complex surface elevation spectrum of the wave field as a function of angular frequency ω and direction θ. Values of $\tilde{u}$, $\tilde{v}$, and $\tilde{w}$ are related to $F(\omega, \theta)$ according to linear wave theory:

$$\tilde{u}(x, y, z, t) = \int_{-\infty}^{\infty}\int_{-\pi}^{\pi} F(\omega, \theta)|\omega|\cos\theta \times K_u e^{i(\omega t - \phi - k_x x - k_y y)}\, d\theta\, d\omega, \quad (8)$$

$$\tilde{v}(x, y, z, t) = \int_{-\infty}^{\infty}\int_{-\pi}^{\pi} F(\omega, \theta)|\omega|\sin\theta \times K_v e^{i(\omega t - \phi - k_x x - k_y y)}\, d\theta\, d\omega, \quad (9)$$

$$\tilde{w}(x, y, z, t) = \int_{-\infty}^{\infty}\int_{-\pi}^{\pi} iF(\omega, \theta)\omega \times K_w e^{i(\omega t - \phi - k_x x - k_y y)}\, d\theta\, d\omega, \quad (10)$$

where

$$K_u = K_v = \frac{\cosh|k|(z + h)}{\sinh|k|h}, \quad (11)$$

$$K_w = \frac{\sinh|k|(z + h)}{\sinh|k|h}, \quad (12)$$

$$|k| = \sqrt{k_x^2 + k_y^2}, \quad (13)$$

where k is the wavenumber vector and h is water depth. Successive depth cell positions along acoustic beams correspond to different horizontal locations. Consequently, the wave-induced portion of the

different along-beam velocity components is not completely in phase. The sums and differences of the wave components at opposing depth cells are defined by

$$\tilde{u}_p = \tilde{u}_1 + \tilde{u}_2 = \int_{-\infty}^{\infty}\int_{-\pi}^{\pi} 2iF(\omega, \theta)(\omega K_w \cos\alpha \cos k_x d - |\omega| K_u \cos\theta \sin\alpha \sin k_x d) e^{i(\omega t - \phi)}\, d\theta\, d\omega, \quad (14)$$

$$\tilde{u}_m = \tilde{u}_1 - \tilde{u}_2 = \int_{-\infty}^{\infty}\int_{-\pi}^{\pi} 2F(\omega, \theta)(\omega K_w \cos\alpha \sin k_x d + |\omega| K_u \cos\theta \sin\alpha \cos k_x d) e^{i(\omega t - \phi)}\, d\theta\, d\omega. \quad (15)$$

Similar expressions hold for $\tilde{v}_p$ and $\tilde{v}_m$. The phase of each of the combined velocity components $\tilde{u}_p$, $\tilde{u}_m$, $\tilde{v}_p$, and $\tilde{v}_m$ is thus depth independent. Power spectra are obtained from (15) and (14) and the analogous equations for $\tilde{v}_p$ and $\tilde{v}_m$:

$$S_{\tilde{u}_p} = \int_{-\pi}^{\pi} 4\omega^2 (K_w \cos\alpha \cos k_x d - K_u \cos\theta \sin\alpha \sin k_x d)^2 \times S_\eta(\omega, \theta)\, d\theta, \quad (16)$$

$$S_{\tilde{u}_m} = \int_{-\pi}^{\pi} 4\omega^2 (K_w \cos\alpha \sin k_x d + K_u \cos\theta \sin\alpha \cos k_x d)^2 \times S_\eta(\omega, \theta)\, d\theta, \quad (17)$$

$$S_{\tilde{v}_p} = \int_{-\pi}^{\pi} 4\omega^2 (K_w \cos\alpha \cos k_y d - K_v \sin\theta \sin\alpha \sin k_y d)^2 \times S_\eta(\omega, \theta)\, d\theta, \quad (18)$$

$$S_{\tilde{v}_m} = \int_{-\pi}^{\pi} 4\omega^2 (K_w \cos\alpha \sin k_y d + K_v \sin\theta \sin\alpha \cos k_y d)^2 \times S_\eta(\omega, \theta)\, d\theta. \quad (19)$$

The depth independence of the phases of $\tilde{u}_p$, $\tilde{u}_m$, $\tilde{v}_p$, and $\tilde{v}_m$ can be used to remove noise and turbulence influences from the combined velocity components. Using the assumption that the velocity fluctuations u'_p, u'_m, v'_p, and v'_m are statistically incoherent throughout the water column, depth averaging of the combined velocity components removes turbulence and noise, for example,

$$\langle u_p \rangle = \langle \tilde{u}_p \rangle, \quad (20)$$

where the angle brackets denote depth averaging. From (20) and the assumption that wave-induced and turbulence or noise fluctuations are statistically independent, it follows that

$$S_{u_p} = S_{\tilde{u}_p} + S_{u'}, \quad (21)$$

and for the cross-spectrum between $\langle u_p \rangle$ and u_p:

$$S_{u_p \langle u_p \rangle} = S_{\tilde{u}_p \langle u_p \rangle}, \quad (22)$$

where the contribution to the cross-spectrum by turbulence and noise is zero.

Using linear wave theory, the coherence between depth mean and local values of u_p is equal to unity:

$$\gamma_{\tilde{u}_p \langle u_p \rangle}^2 = \frac{|S_{\tilde{u}_p \langle \tilde{u}_p \rangle}|^2}{S_{\tilde{u}_p} S_{\langle u_p \rangle}} = 1. \quad (23)$$

Substitution of (21), (22), and (23) into the definition of coherence between the local and depth-mean velocity components results in

$$\gamma_{u_p \langle u_p \rangle}^2 = \left(1 + \frac{S_{u'_p}}{S_{\tilde{u}_p}}\right)^{-1} = \frac{S_{\tilde{u}_p}}{S_{u_p}}. \quad (24)$$

The wave-induced contribution to spectra of the combined velocity component can be calculated as in

$$S_{\tilde{u}_p} = \gamma_{u_p \langle u_p \rangle}^2 S_{u_p}. \quad (25)$$

Local and depth mean values of the combined velocity components are readily calculated from the ADCP measurements of u_1, u_2, v_1, and v_2.

The surface elevation spectrum $S_{\tilde{\eta}}$ can be calculated from the power spectra (16), (17), (18), and (19):

$$S_{\tilde{\eta}} = \frac{S_{\tilde{u}_p} + S_{\tilde{u}_m} + S_{\tilde{v}_p} + S_{\tilde{v}_m}}{8\omega^2 K_w^2 \cos^2\alpha + 4\omega^2 K_u^2 \sin^2\alpha}. \quad (26)$$

The redundant information available from different ADCP depth cell heights can be capitalized by fitting a linear line through a plot of denominator values versus numerator values, forced through the origin. The slope of the regression line then provides the estimate of $S_{\tilde{\eta}}$.

3. Field experiment and data processing

Field data were collected in 13-m-deep water off the coast of Noordwijk, Netherlands, with an RDI 1.2-MHz ADCP and a collocated Datawell Waverider buoy. The ADCP employs a Janus configuration, consisting of four acoustic transducers looking outward from the instrument central axis at an angle $\alpha = 20°$. The -3 dB width of the beams is about 1.4°. The depth cell size ℓ was chosen 1 m, resulting in a blanking distance of 1.54

m above the transducer. The self-contained ADCP sampled in bursts of 20 min, once every hour in fast-pinging mode 12, each ping being an average over eight subpings. The instrument was attached to a bottom-mounted iron frame such that the ADCP transducers were at 0.4 m above the local seafloor. Mean and minimal water depths over the time span of a burst were calculated using an attached pressure transducer. The ADCP data storing was intermittently disturbed due to malfunctioning of a CompactFlash memory card, resulting in several data gaps in the data series. In total, 137 valid 20-min bursts were recorded.

The wave buoy sampled at 1.28 Hz over burst intervals synchronous to the ADCP. The ADCP sampled at 1.25 Hz, which is the optimal setting closest to 1.28 Hz for mode-12 measurements, ensuring a low noise level (Williams and Simpson 2004). Wave buoy and ADCP data series were preprocessed analogously to remove spikes and low-frequency oscillations. Spikes were removed based on a 4σ test. Low-frequency oscillations, which primarily have a tidal origin, were high-pass filtered according to Rijkswaterstaat conventions using a symmetric moving average filter. For 1.28- and 1.25-Hz data series the filter implied a turnover frequency at 31.5 and 30.7 mHz, respectively.

The sampled 20-min intervals were divided in six subseries of 256 samples, where 0 and 8 samples overlap for the wave buoy and ADCP subseries, respectively. After applying a 10% cosine tapering window, subseries were FFTed and averaged. The high-pass filter has a small influence in the frequency domain above the turnover frequency, which was accounted for by multiplying the obtained energy density spectra with the appropriate correction function C:

$$C = \left\{1 - \left[\frac{\sin(0.5M\omega/f_s)}{M\sin(0.5\omega/f_s)}\right]^4\right\}^{-2}, \tag{27}$$

where $M = 13$ is filter width and f_s denotes sample frequency. The corrected spectral arrays were convoluted with vector [0.25, 0.5, 0.25] to guarantee further smoothing in the frequency domain and the resolution was decreased to 10 mHz.

To observe differences in ADCP performance under more or less energetic conditions, the burst periods were subdivided in two categories. For each burst period the significant wave height H_{m0} was calculated according to

$$H_{m0} = 4\sqrt{\int_{0.03}^{0.5} S_{\tilde{\eta},\mathrm{meas}}(f)\,df}, \tag{28}$$

where $S_{\tilde{\eta},\mathrm{meas}}(f)$ denotes the wave-buoy-derived surface elevation spectrum. The two categories correspond to $H_{m0} < 1.5$ m, representing nonenergetic conditions for which 121 burst periods were available, and to $H_{m0} > 1.5$ m, representing energetic conditions for which 16 burst periods were available.

4. Comparisons

Surface elevation spectra from ADCP velocity and wave buoy measurements are compared in Fig. 1. At frequencies between 0.12 and 0.2 Hz, where most energy density is concentrated, the general agreement between ADCP and wave buoy estimates of $S_{\tilde{\eta}}$ is very good (Fig. 1). In Fig. 1a, corresponding to a burst with relatively little high-frequency energy, the ADCP energy is well under that of the wave buoy, whereas the relatively energetic ADCP and wave buoy spectra in Fig. 1d are in good agreement, even at the higher frequencies. Figure 2 shows $\gamma_{u_p}\langle u_p\rangle^2$ as a function of frequency for lowermost and uppermost depth cells in burst periods corresponding to those in Fig. 1, illustrating the frequency-dependent fraction of wave energy contained in oscillation of filtrated ADCP velocity data. Values of $\gamma_{u_p}\langle u_p\rangle^2$ can reduce to values as low as 0.2, especially for depth cells close to the seafloor (Fig. 2).

Figure 1 also includes the ADCP spectra that were calculated without applying the filtration method. It appears that removal of the significant portion of depth-incoherent oscillation does not clearly reduce the differences between ADCP and wave buoy surface elevation spectra. For the nonenergetic burst period displayed in Fig. 1a, spectral energy density at relatively high frequencies between 0.3 and 0.5 Hz is even more strongly underestimated when the velocity data are filtrated. From the ADCP data an independent prediction of the surface elevation spectrum can be derived for every depth cell height, which can be used to investigate the self-consistency of ADCP spectral energy estimates. Scatterplots of numerator versus denominator values of the fraction in Eq. (26) show that the filtration does improve the self-consistency of the ADCP wave data, as linear lines through the origin fit better to the scatter points pertaining to filtrated data (Fig. 3). Only at very high frequencies does the filtration alter the slope of the regression line forced through the origin, resulting in a significantly different overall ADCP estimate of spectral energy density.

The fact that the improved self-consistency of the ADCP spectra resulting from filtration does not result in a closer agreement with the wave buoy spectra may relate to the intrinsic variability in the wave field and to the error in the wave buoy measurements. The intrinsic variability in the wave field causes differences because

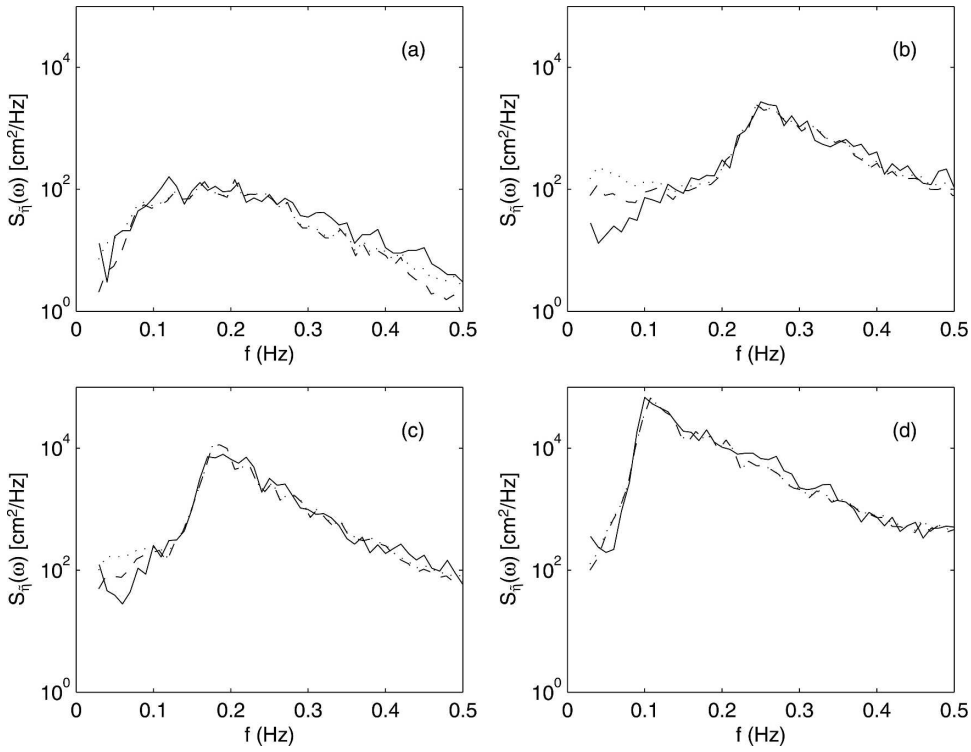

FIG. 1. Comparison of surface elevation spectra predicted from filtrated (dashed lines) and unfiltrated (dotted lines) ADCP velocity measurements and from wave buoy measurements (solid lines) during contrasting conditions. Corresponding values of H_{m0} are (a) 0.19, (b) 0.62, (c) 1.08, and (d) 2.64 m.

the wave buoy and the ADCP were almost, but not exactly, located at the same position. This is particularly relevant for high-frequency waves with a short wavelength. Not filtrating the data may bring the ADCP spectra incidentally closer to the wave buoy spectra, but for the wrong reason, by compensating a high-frequency energy deficit with energy density caused by noise and turbulence. ADCP spectra based on filtrated data are therefore preferred over the ADCP spectra from nonfiltrated data, and are further analyzed in the remainder of this section.

The general performance of the ADCP for measurement of surface elevation spectra can be established from Fig. 4, which shows the normalized root-mean-square error (NRMSE), defined as

$$\mathrm{NRMSE}(f) = \frac{\sqrt{\sum_{j=1}^{N} [S_{\tilde{\eta},\mathrm{pred}}(f) - S_{\tilde{\eta},\mathrm{meas}}(f)]_j^2}}{\sqrt{\sum_{j=1}^{N} [S_{\tilde{\eta},\mathrm{meas}}(f)]_j^2}}. \tag{29}$$

Herein, $S_{\tilde{\eta},\mathrm{pred}}(f)$ denotes the ADCP-derived surface elevation spectrum and N is the number of 20-min bursts. At frequencies between 0.08 and 0.5 Hz, the NRMSE varies between 0.2 and 0.3 both for the energetic and the nonenergetic burst periods. At frequencies in between 0.03 and 0.08 Hz, the NRMSE is significantly higher, especially for the nonenergetic burst periods. The NRMSE could be further reduced by additional smoothing in the frequency space, which would compromise the frequency resolution. It is noted that error in the wave buoy estimates of the surface elevation spectrum and the effect of the intrinsic variability in the wave field are falsely attributed to ADCP error.

To investigate a possible bias, a normalized gain function $G(f)$ was calculated, defined as

$$G(f) = \left[\frac{S_{\tilde{\eta},\mathrm{pred}}(f)}{S_{\tilde{\eta},\mathrm{meas}}(f)}\right]^{1/2}. \tag{30}$$

Considering conditions when $H_{m0} > 1.5$, the mean and median normalized gain deviate less than 0.15 from unity at frequencies between 0.08 and 0.5 Hz (Fig. 5). Considering burst periods when $H_{m0} < 1.5$, $G(f)$ decreases approximately linearly with f, amounting to 0.8 at $f = 0.5$ Hz. Under nonenergetic conditions, an underestimation of high-frequency surface elevation oscillation is hence observed up to 20%. In part, this relates

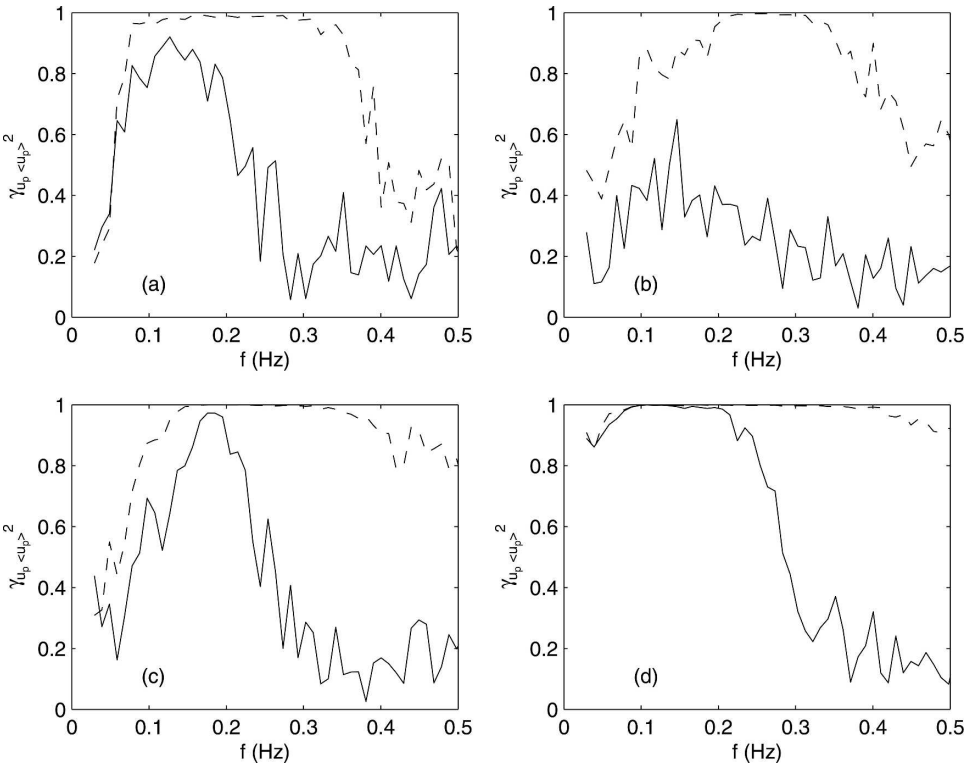

FIG. 2. Coherence between depth mean and local variation of u_p. For dashed and solid lines local variation of u_p corresponds to the ADCP depth cell closest to the seafloor and closest to the water surface, respectively. Values of $\gamma_{u_p\langle u_p\rangle}\langle u_p\rangle^2$ can be interpreted as the fraction of energy contained in u_p oscillation induced by surface gravity waves. Coherence functions and surface elevation spectra in Figs. 1 and 2 pertain to corresponding burst periods.

to the horizontal width of the sample volumes, which increases with distance from the transducer. The appendix shows that horizontal averaging can explain an amplitude reduction of maximally 1.5% at 0.5 Hz. The effect of vertical averaging over the depth cell height, which may introduce a bias due to the nonlinear depth dependence of K_u, K_v, and K_w, is an order of magnitude smaller. The calibration uncertainty of the wave buoy may explain another part of the observed bias.

In the low-frequency band in between 0.03 and 0.12 Hz, ADCP and wave buoy estimates of surface elevation spectral estimates diverge substantially more than in the remainder of the considered frequency domain (Figs. 1 and 2). The ADCP velocity measurements contain an excess amount of energy density, indicating that only part of the velocity oscillation at swell wave frequencies is induced by surface gravity waves. Figure 2 shows that the coherence of u_p oscillation over depth is low at swell wave frequencies, where even local u_p oscillation near the surface coheres weakly with depth-averaged variation of u_p. Large-scale turbulent motions could provide an explanation for this incoherent behavior. The gain bias is, however, caused by the depth-coherent part in variation of the combined velocity components.

Figure 6 shows surface elevation spectral estimates as a function of the elevation of the used ADCP depth cell above the seafloor for three synoptic frequencies. Estimates of $S_{\bar{\eta}}(f)$ are self-consistent at $f = 0.16$ Hz, which is generally the case at frequencies higher than 0.12 Hz provided that conditions are sufficiently energetic. Estimates $S_{\bar{\eta}}(f)$ in the low-frequency band between 0.03 and 0.12 Hz are larger if a depth cell around middepth has been used, indicating an excess of spectral density of ADCP velocity in this region. The energy density peaks at middepth suggest the prevalence of internal waves, which may be generated by isolated topographic features (Hibiya 1986; Baines 1995) or be resonant waves trapped to the bed topography (Pietrzak et al. 1990). Internal waves have periods typically in the order of hours, but frequencies as high as the buoyancy frequency

$$N = \sqrt{\frac{g}{\rho}\frac{d\rho}{dz}} \tag{31}$$

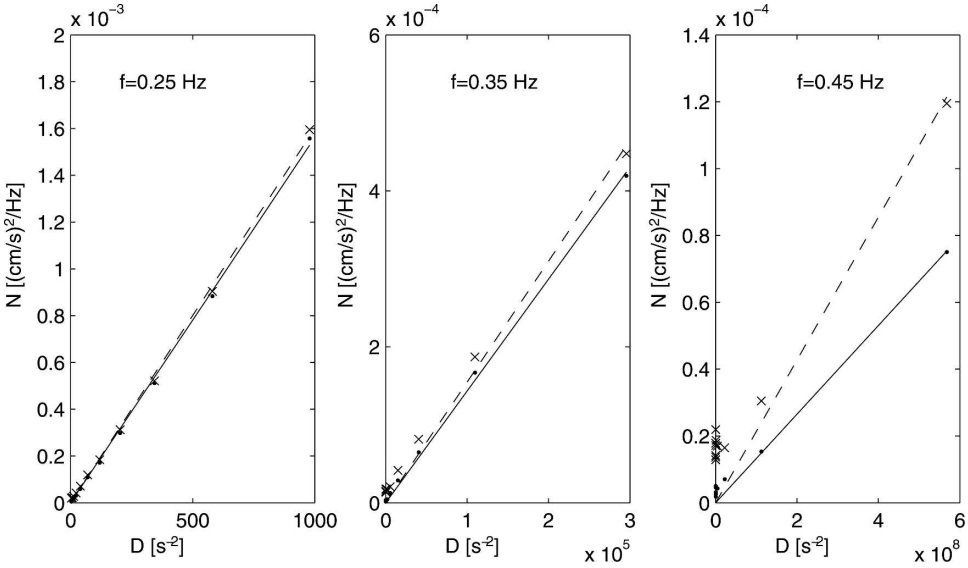

FIG. 3. Plots of denominator values vs numerator values of the fraction in Eq. (26), for ADCP data corresponding to Fig. 1a ($D = 8\omega^2 K_w{}^2 \cos^2\alpha + 4\omega^2 K_u{}^2 \sin^2\alpha$; $N = S_{\tilde{u}_p} + S_{\tilde{u}_m} + S_{\tilde{v}_p} + S_{\tilde{v}_m}$). The slope of the regression line through the origin equals the estimate $S_{\tilde{\eta}}$. Dots and solid lines correspond to filtrated data; crosses and dashed lines correspond to the nonfiltrated data. Filtrated data points show less scatter around a linear regression line through the origin, indicating a higher self-consistency of the ADCP surface elevation spectral estimates.

may occur, where ρ denotes seawater density. The observational site is located in the North Sea at the latitude of Noordwijk, which is under the direct influence of the pulsing Rhine outflow. A buoyancy frequency of 0.4 Hz would require a vertical density gradient of 0.17 kg m^{-3} m^{-1} at an ambient density of 1025 kg m^{-3}, which is a realistic degree of stratification for the region (De Ruijter et al. 1992; Souza and Simpson 1997).

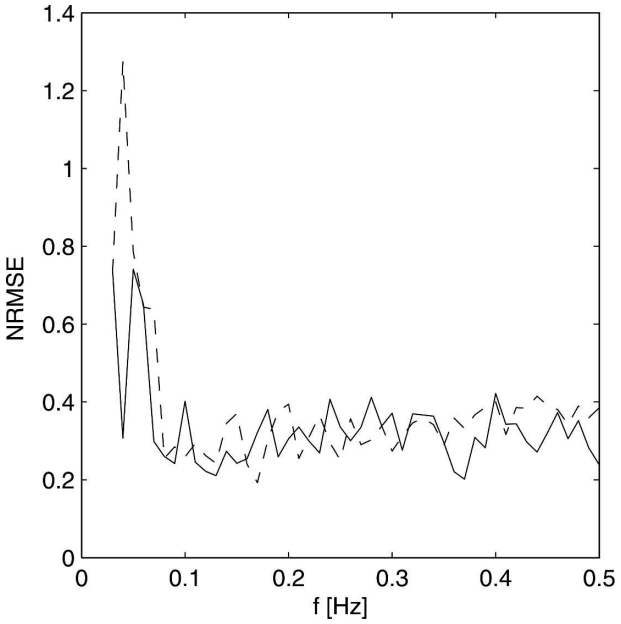

FIG. 4. NRMSE as a function of frequency. Dashed line and solid line correspond to NRMSE calculations over burst periods for which $H_{m0} < 1.5$ m and $H_{m0} > 1.5$ m, respectively.

5. Discussion

The proposed linear filtration technique is in some respect analogous to existing linear filtration techniques using cross-spectra of pressure and current velocity to separate orbital wave velocities and turbulence (Kitaigorodskii et al. 1983; Terray and Bliven 1985; Cheung and Street 1988; Green 1992). These techniques use the assumption that the coherence between $\tilde{p}$ or $\tilde{\eta}$ and $\tilde{u}$ or $\tilde{v}$ is unity, which neglects the influence of directional spreading (Kitaigorodskii et al. 1983; Herbers et al. 1991). The coherence function $\gamma_{\tilde{u}_p}\langle_{\tilde{u}_p}\rangle^2$ [Eq. (23)] is independent of directional spread. However, there is no complete certainty that the depth coherent part of the ADCP estimates of u_p can be entirely ascribed to wave oscillation. Figure 2 shows that the $\gamma_{u_p}\langle_{u_p}\rangle^2$ can deviate significantly from unity even for local variation of u_p near the surface, where orbital wave velocity is highest. Strong turbulence may have a circumstantial depth coherent component, which is falsely attributed to wave oscillation. This would imply an overestimation of spectral energy density especially at higher frequencies, whereas a small underestimation

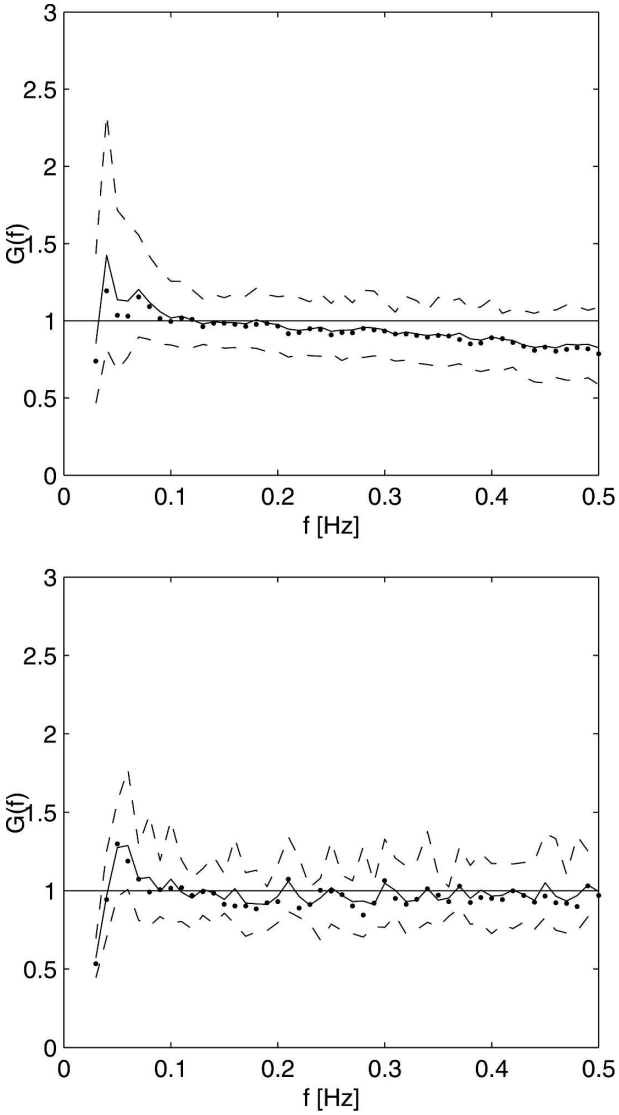

FIG. 5. Estimates of the normalized gain function $G(f)$ [see Eq. (30)]. (top) Burst periods for which $H_{m0} < 1.5$ m. (bottom) Burst periods for which $H_{m0} > 1.5$ m. Solid and dotted lines indicate the mean and median values, respectively. Dashed lines indicate 5% and 95% quantiles.

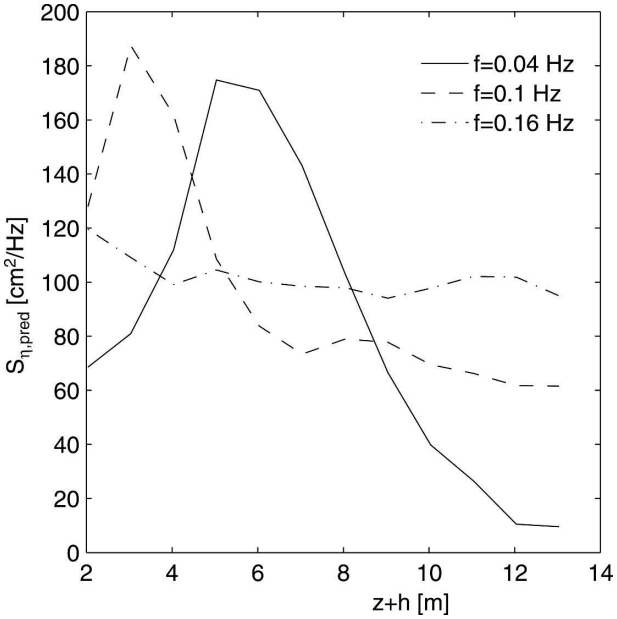

FIG. 6. Surface elevation spectral estimates at three frequencies as a function of the elevation of the used ADCP depth cells above the seafloor. For $f = 0.16$ Hz the ADCP spectral estimates are self-consistent. For $f = 0.1$ Hz and $f = 0.04$ Hz, the spectral estimates are inconsistent, which is caused by an excess of energy density in ADCP velocity around middepth. This suggests a contribution of internal waves.

is observed at these higher frequencies (Fig. 5). This, and the fact that filtrating the ADCP data does not reduce differences between ADCP and wave buoy surface elevation spectra, shows that noise and turbulence are not the limiting factors for ADCP performance regarding wave measurements.

The predominantly high level of agreement between wave-buoy- and ADCP-derived surface elevation spectra confirms previous studies in support of ADCP wave measurements (Terray et al. 1990; Rørbæk and Anderson 2000; Jeans et al. 2003; Shih et al. 2003), which are generally based on integrated spectral parameters like H_{m0} and T_{m02}. Although in the present study the removal of the depth-incoherent part of the velocity oscillation did not yield a closer agreement between wave buoy and ADCP spectra, this may be different in shallow waters closer to the coast where flows are stronger and turbulence levels higher. The methodology presented herein could be extended to improving estimates of directional properties such as mean direction and directional spread. Directional spreading estimates from ADCPs may be particularly sensitive to noise and benefit from the noise reduction technique. Using existing techniques such as the iterative maximum likelihood method (Pawka 1983; Krogstad et al. 1988) or the maximum entropy method (Massel 1996), the directional estimates can be derived from $\tilde{u}_p$, $\tilde{u}_m$, $\tilde{v}_p$, and $\tilde{v}_m$. Time series of these variables can be obtained by filtrating the discrete Fourier transforms of u_p, u_m, v_p, and v_m with the methodology explained in section 2, and by taking the inverse discrete Fourier transform of the obtained result.

The present analysis spans a limited range of conditions, but there are no inherent uncertainties in using ADCP velocity, which limits its applicability in more energetic seas. The encountered field conditions included tidal currents up to 0.7 m s^{-1}, which may modify the linear dispersion relation (Kirby and Chen 1989),

here used to calculate $|k|$. Tests were performed to leave $|k|$ as an unknown in the calculations to be solved using a least squares fit, which generally showed minor differences with estimates of $|k|$ using the linear dispersion relation. The tidal currents at the experimental site were rarely aligned with the wave propagation direction. In situations where waves do propagate along the tidal principal axis, the option to leave $|k|$ as an unknown may be valuable.

The observed inconsistency of ADCP estimates of low-frequency energy density, which appeared from using different depth cells for the spectrum calculation (Fig. 6), demonstrates the physical limitations of estimating surface elevation spectra from current velocity. Herbers et al. (1991) found normalized gain anomalies comparable to those in Fig. 5, which they attributed to contamination of the received sound caused by reflections from the sea surface. Sidelobes contaminate the ADCP signals especially in case of a smooth sea surface, acting as a mirror to relatively weak sidelobes that are directed nearly vertically upward (Gordon 1996; Medwin and Clay 1998). The low-frequency energy excess observed in ADCP velocity cannot be ascribed to sidelobe effects, as no anomalies were found in the raw velocity data. Internal waves provide a plausible explanation, but to the authors' knowledge no field evidence exists showing that internal wave energy disturbs swell wave measurement in coastal regions. Existing studies on the interaction between surface and internal waves are focused on oceanic or offshore environments (Hughes 1978; Gotwols et al. 1988; Watson 1990; Van Haren 2005), where the buoyancy frequency is in the frequency range of tides.

Another explanation for the depth variation of low-frequency energy density may be the nonlinear kinematics of the wave field. Putrevu and Svendsen (1995) present a theoretical solution for the vertical structure of the velocity profiles under infragravity waves. They show that the velocity with local forcing of infragravity waves has a substantial vertical structure. It is well possible that infragravity waves may not be measured by the moored wave buoy. The ADCP may provide an ideal means to study velocity profiles under infragravity wave motion.

6. Conclusions

ADCP wave measurements of orbital velocity can be combined to yield velocity components whose discrete Fourier transforms contain depth-independent phases. Depth averaging of those combined components removes instrumental noise and turbulence, as far as turbulence is depth incoherent. Using this principle, a linear filtration technique is presented to separate wave-induced orbital velocity from turbulence and noise in the combined components. For each ADCP depth cell height an independent estimation of the surface elevation spectrum can be obtained from the filtrated data, which allows one to investigate the self-consistency of the ADCP spectral energy density estimates.

A field experiment was carried out in 13-m-deep water with a bottom-mounted 1.2-MHz ADCP and a collocated wave buoy for verification. The ADCP operated in mode 12 at 1.25 Hz, with 1-m depth cells. Filtrated and nonfiltrated ADCP velocity measurements were converted to surface elevation spectra and compared with corresponding wave-buoy-derived spectra. The part of depth-incoherent velocity oscillation in the ADCP velocity data was significant, especially for velocity measurements close to the bed and for high-frequency velocity oscillation. The surface elevation spectra derived from filtrated and nonfiltrated ADCP data compared similarly well to the wave buoy spectra. Differences between spectra based on filtrated and nonfiltrated data were small compared to spectral differences that may have been caused by the intrinsic variability of the wave field and error in the wave buoy measurements. Filtrating the ADCP data did improve the self-consistency of the ADCP wave measurements, meaning that surface elevation spectra derived from ADCP velocity estimates close to the bed were in closer agreement with spectra derived from ADCP velocity estimates close to the surface.

In the swell wave frequency band the surface elevation spectral estimates from ADCP velocity diverge significantly from corresponding wave buoy estimates. The spectral estimates from velocity variation at mid-depth regularly contain an excess of spectral energy density. Internal waves may have frequencies comparable to the local buoyancy frequency, which may enter the swell wave frequency domain in case of strong stratification. The location of the experimental site is in the region of freshwater influence of the Rhine, where the required degree of stratification is often prevalent. Internal waves may thus provide an unconventional explanation for the excess of energy density in velocity spectra at swell wave frequencies.

Acknowledgments. This research was funded by the National Institute for Coastal and Marine Management/RIKZ, Rijkswaterstaat (Netherlands). P. J. J. F. Torfs (Wageningen University), B. G. Ruessink, and P. Hoekstra (Utrecht University) are acknowledged for their contribution to this paper. M. C. G. van Maarseveen (Utrecht University) and B. Strong (RD Instruments) are thanked for technical support.

APPENDIX

Attenuation of Velocity Estimates Caused by Horizontal Averaging

Raw data ADCP velocity measurements can be considered as an average over the depth cell volume. The present appendix gives details about the effect of averaging over the horizontal width of the sample volume. The width that a sample volume spans, denoted as Δx, can be approximated as

$$\Delta x \approx \ell \tan\alpha + (z + h)\phi, \tag{A1}$$

where ϕ is beamwidth. Rather that u_1, the ADCP observes a convoluted signal $\hat{u}_1$, which reads

$$\hat{u}_1 = \int_{-\infty}^{\infty} u_1(x - \xi) I(\xi)\, d\xi, \tag{A2}$$

where

$$I(\xi) = \frac{1}{\Delta x} \quad \text{for} \quad |\xi| \le \Delta x/2$$
$$= 0 \text{ elsewhere.} \tag{A3}$$

Fourier transforms of u_1, $\hat{u}_1$ and I relate as

$$\mathcal{F}[\hat{u}_1] = \mathcal{F}[u_1]\mathcal{F}[I], \tag{A4}$$

where the modulus of $\mathcal{F}[I]$ is readily obtained

$$|\mathcal{F}[I]| = \frac{1}{\Delta x}\left| \int_{d-\frac{1}{2}\Delta x}^{d+\frac{1}{2}\Delta x} e^{-ik_x x}\, dx \right| = \left| \frac{\sin\left(\frac{1}{2} k_x \Delta x\right)}{\frac{1}{2} k_x \Delta x} \right|. \tag{A5}$$

Values of $|\mathcal{F}[I]|$ can be interpreted as the attenuation factor due to horizontal averaging over a depth cell, as a function of the x component of the wavenumber. Using the linear dispersion relation and presuming that waves travel along the x direction, $|\mathcal{F}[I](k_x)|$ can be transformed to $|\mathcal{F}[I](f)|$. In the frequency range between 0.03 and 0.5 Hz, the attenuation factor increases progressively with frequency. For the present configuration with $\ell = 1$ m, $\alpha = 20°$, and $\phi = 0.0244$ rad, and taking $h = 10$ m and $z = 0$ m, the attenuation factor amounts to 1.5% at 0.5 Hz. This demonstrates that merely a small bias in high-frequency ADCP measurements can be attributed to horizontal averaging.

REFERENCES

Baines, P., 1995: *Topographic Effects in Stratified Flows.* Cambridge University Press, 482 pp.

Bowden, K. F., and R. A. White, 1966: Measurements of the orbital velocities of sea waves and their use in determining the directional spectrum. *Geophys. J. Roy. Astron. Soc.,* **12,** 33–54.

Brumley, B. H., R. G. Cabrera, K. L. Deines, and E. A. Terray, 1983: Performance of a broadband acoustic Doppler current profiler. *J. Oceanic Eng.,* **16,** 402–407.

Cheung, T. K., and R. L. Street, 1988: The turbulent layer in the water at an air-water interface. *J. Fluid Mech.,* **194,** 133–151.

De Ruijter, W. P. M., A. V. D. Giessen, and F. C. Groenendijk, 1992: Current and density structure in the Netherlands coastal zone. *Dynamics and Exchanges in Estuaries and the Coastal Zone,* D. Prandle, Ed., Amer. Geophys. Union, 529–550.

Gordon, R. L., 1996: Acoustic Doppler current profilers, principles of operation, a practical primer. RD Instruments Tech. Rep., P/N 951-6069-00, 52 pp.

Gotwols, B. L., R. E. Sterner, and D. R. Thompson, 1988: Measurement and interpretation of surface-roughness changes induced by internal waves during the joint Canada–United States ocean wave investigation project. *J. Geophys. Res.,* **93,** 12 265–12 281.

Green, M. O., 1992: Spectral estimates of bed shear stress at subcritcal Reynolds number in a tidal boundary layer. *J. Phys. Oceanogr.,* **22,** 903–917.

Herbers, T. H. C., R. L. Lowe, and R. T. Guza, 1991: Field verification of acoustic Doppler surface gravity wave measurements. *J. Geophys. Res.,* **96,** 17 023–17 035.

Hibiya, T., 1986: Generation mechanism of internal waves by tidal flow over a sill. *J. Geophys. Res.,* **91,** 7696–7708.

Hughes, B. A., 1978: Effect of internal waves on surface wind waves. 2. Theoretical-analysis. *J. Geophys. Res.,* **83,** 455–465.

Jeans, G., C. Primrose, N. Descusse, B. Strong, and P. van Weert, 2003: A comparison between directional wave measurements from the RDI Workhorse with Waves and the Datawell Directional Waverider. *Proc. IEEE/OES Seventh Working Conf. on Current Measurement Technology,* San Diego, CA, IEEE/OES, 148–152.

Kirby, J. T., and T. M. Chen, 1989: Surface waves on vertically sheared flows: Approximate dispersion relations. *J. Geophys. Res.,* **94,** 1013–1027.

Kitaigorodskii, S. A., M. A. Donelan, J. L. Lumley, and E. A. Terray, 1983: Wave-turbulence interactions in the upper ocean. Part II: Statistical characteristics of wave and turbulent components of the random velocity field in marine surface layer. *J. Phys. Oceanogr.,* **13,** 1988–1999.

Krogstad, H. E., R. L. Gordon, and M. C. Miller, 1988: High-resolution directional wave spectra from horizontally mounted acoustic Doppler current meters. *J. Atmos. Oceanic Technol.,* **5,** 340–352.

Lhermitte, R., and R. J. Serafin, 1984: Pulse to pulse coherent Doppler sonar signal processing techniques. *J. Atmos. Oceanic Technol.,* **1,** 293–308.

Longuet-Higgins, M. S., D. E. Cartwright, and N. D. Smith, 1963: Observations of the directional spectrum of sea waves using the motions of a floating buoy. *Ocean Wave Spectrum,* Prentice-Hall, 111–136.

Massel, S. R., 1996: *Ocean Surface Waves: Their Physics and Prediction.* Advanced Series on Ocean Engineering, Vol. 11, World Scientific, 491 pp.

Medwin, H., and C. S. Clay, 1998: *Fundamentals of Acoustical Oceanography.* Academic Press, 712 pp.

Nagata, Y., 1964: The statistical properties of orbital wave motions and their application for the measurement of directional wave spectra. *J. Oceanogr. Soc. Japan,* **19,** 169–181.

Pawka, S. S., 1983: Island shadows in wave directional spectra. *J. Geophys. Res.,* **88,** 2579–2591.

Pietrzak, J. D., C. Kranenburg, and G. Abraham, 1990: Resonant internal waves in fluid flow. *Nature,* **344,** 844–847.

Putrevu, U., and I. A. Svendsen, 1995: Infragravity velocity profiles in the surf zone. *J. Geophys. Res.,* **100,** 16 131–16 142.

Rørbæk, K., and H. Anderson, 2000: Evaluation of wave measurements with an acoustic Doppler current profiler. *Proc. Oceans 2000,* Providence, RI, MTS/IEEE, 1181–1187.

Shih, H. H., M. Bushnell, K. Tronvig, and T. Mero, 2003: Wave and current measurements in the Chesapeake Bay. *Proc. IEEE/OES Seventh Working Conf. on Current Measurement Technology,* San Diego, CA, IEEE/OES, 264–270.

Souza, A. J., and J. H. Simpson, 1997: Controls on stratification in the Rhine RPFI system. *J. Mar. Syst.,* **12,** 311–323.

Terray, E. A., and L. F. Bliven, 1985: The vertical structure of turbulence beneath gently breaking wind waves. *The Ocean Surface,* Y. Toba and H. Mitsuyasu, Eds., Reidel, 395–400.

——, H. E. Krogstad, R. Cabrera, R. L. Gordon, and A. Lohrmann, 1990: Measuring wave direction using upward-looking Doppler sonar. *Proc. IEEE Fourth Working Conf. on Current Measurement,* Clinton, MD, IEEE, 252–257.

Theriault, K. B., 1986: Incoherent multibeam Doppler current profiler performance. I. Estimate variance. *IEEE J. Oceanic Eng.,* **OE-11,** 7–15.

Van Haren, H., 2005: Internal waves near the buoyancy frequency in a narrow waveguide. *Neth. J. Sea Res.,* **53,** 121–129.

Watson, K. M., 1990: The coupling of surface and internal gravity-waves—Revisited. *J. Phys. Oceanogr.,* **20,** 1233–1248.

Williams, E., and J. H. Simpson, 2004: Uncertainties in estimates of Reynolds stress and TKE production rate using the ADCP variance method. *J. Atmos. Oceanic Technol.,* **21,** 347–357.